

# Cooling slope casting of cast iron

## Abkühlkurve beim Gießen von Gusseisen

A. M. Negm<sup>1</sup>, Sayed A. Abdallah<sup>2</sup>, M. Ibrahim<sup>3</sup>, T. S. Mahmoud<sup>4</sup>

The aim of the present work is to study the effect of semi-solid processing using cooling slope method on the microstructure and mechanical properties of grey cast iron. A water cooled castable cement coated steel plate with a variable inclination angle is used to make a mechanical treatment on the semi-solid flow of grey cast iron. The experiment is repeated for three different pouring temperatures and three inclination angles. The tensile test, hardness test and microstructure examination is used to compare the new properties of the new resulting grey cast irons. The results show that the sharp edged carbon flakes can be refined and the mechanical properties is enhanced. The carbon particles average circularity is increased followed with a decrease in carbon particle size due to the effect of the cooling plate.

**Keywords:** Semi-solid / cooling slope / grey cast iron / carbon flakes / steel plate

**Schlüsselwörter:** Halbfest / Abkühlkurve / Grauguss / Kohlenstoffflakes / Stahlplatte

### 1 Introduction

At the point when concentrating on the microstructure of the gray cast iron it is obviously that there are countless micro cracks that originate from the sharp edges of carbon flakes. The carbon flakes come about because of carbon separation from the solidified iron due to diffusion. As a result the researchers issue was the means by which to change the shape of the carbon flakes to a less sharp edged states of graphite. The change in the microstructure of cast iron originates from the trace elements, the addition of alloying elements, the modification of solidification behavior, and heat treatment after sol-

idification to produce the desired mechanical properties.

The chemical composition of cast iron fluctuates fundamentally relying upon the grade of pig iron utilized as a part of its manufacturing. Cast iron contains carbon in the range of ~2 to 4 weight percentage. The mode and concentration of carbon in the cast iron is controlled to deliver different grades of cast iron, which vary altogether in their mechanical properties and weldability. The carbon equivalent of cast iron helps to recognize the grey cast iron type, and microstructure. The carbon equivalent is characterized in Equation (1) [1].

<sup>1</sup> Mechanical Engineering Department, Modern Academy for Engineering and Technology, Cairo, 11585, Egypt

<sup>2</sup> Mechanical Engineering Department, Shoubra Faculty of Engineering, Benha University, Cairo, 13512, Egypt

<sup>3</sup> Mechanical Engineering Department, Shoubra Faculty of Engineering, Benha University, Cairo, 13512, Egypt

<sup>4</sup> Mechanical Engineering Department, Shoubra Faculty of Engineering, Benha University, Cairo, 13512, Egypt

Corresponding author: A. M. Negm, Mechanical Engineering Department, Modern Academy for Engineering and Technology, Cairo, 11585, Egypt, E-Mail: anegm8747@gmail.com

$$CE = \%(\text{carbon}) + 0.33(\% \text{silicon}) + 0.33(\% \text{phosphorus}) - 0.027(\% \text{manganese}) + 0.4(\% \text{sulfur}) \quad (1)$$

A ternary phase diagram of iron-carbon-silicon (Fe-C-Si) is used to describe the solidification behavior because of the existence of silicon in grey cast iron which changes the extent and position of the regions of the iron-iron carbide (Fe-Fe<sub>3</sub>C) binary diagram [2]. When solidification from the melt is finished, the precipitated phase is implanted in a matrix of austenite that has an equilibrium carbon concentration of ~2 weight percentage. On further cooling, the carbon concentration of the austenite diminishes as more cementite or graphite precipitates from solid solution. For conventional cast irons, the austenite then breaks down into pearlite at the eutectoid temperature. In grey cast iron, in any case, if the cooling rate through the eutectoid temperature is adequately slow, then a totally ferritic matrix is gotten, with the excess carbon being deposited on the already existing graphite [1]. The nodular cast iron is produced to avoid the problems of flake shape of graphite in gray cast iron by addition of small amount of magnesium with other elements present in complex alloys. The addition of magnesium removes oxygen and sulfur like impurities which decrease the surface tension of the molten iron by segregation in the melt furnace [3].

One of the new methods to enhance the material properties is semi-solid processing. In 1971 a new semi-solid processing technique called rheocasting was invented. Other methods of semi-solid processing was performed later like thixofforming, thixomoulding, rheomoulding, and cooling slope casting [4,5]. These methods showed a great result in mechanical properties when breaking the dendritic form of materials microstructure and refinement of material grains [6]. The cooling slope casting method is used in this study to get a new grey cast iron type with a lower number of carbon flakes and dendritic forms. This is done by transforming these sharp edged shapes into a circular like shapes. This technique is preferred for its simplicity, productivity, and low cost if compared with the abovementioned other casting methods. To know the best conditions for the cooling slope technique this study is performed on the effect of changing the pouring temperature and the angle

of the cooling slope plate on the properties of grey cast iron.

## 2 Experimental work

A grey cast iron with the chemical composition of (3.5% carbon, 1.81% silicon, 0.719% manganese, 0.1% phosphorus, and 0.02% sulfur) is prepared. The carbon equivalent of this alloy is calculated to know the melting temperature using these composition percentages by substituting in equation 1. The calculated carbon equivalent is 4.119% and the melting temperature is calculated using iron carbon diagram to be 1170 °C. In this experiment the metal is poured on a temperature higher than the melting temperature by (30 °C, 70 °C, and 110 °C) with a tolerance of 10 °C, *Table 1*. The used cooling plate material is steel coated with a layer of castable cement which contains 80% aluminum oxide to get a good cooling rate as it has a thermal conductivity of 1.27 W/(m.k) and thickness of 10 mm. The cooling plate is water cooled to maintain the original room temperature after casting several specimens, *Figure 1*. As a result there is an ability to cast a lot of specimens without waiting the plate to cool down. The cooling plate is inclined with a three different inclination angles (30°, 40°, and 50°) to test the effect of changing the cooling rate during the metal flow along the plate. The plate is coated with a thin layer from graphite above the castable cement coating. The graphite coating is used to prevent sticking of the semi-solid slurry on the castable cement coating.

**Table 1.** Specimens casting parameters and coding.

| no. | code | tilt angle ( $\alpha$ ) | pouring temperature (Tp) |
|-----|------|-------------------------|--------------------------|
| 1   | A    | 30                      | 1278                     |
| 2   | B    | 30                      | 1232                     |
| 3   | C    | 30                      | 1200                     |
| 4   | D    | 40                      | 1275                     |
| 5   | E    | 40                      | 1240                     |
| 6   | F    | 40                      | 1212                     |
| 7   | G    | 50                      | 1260                     |
| 8   | H    | 50                      | 1238                     |
| 9   | I    | 50                      | 1200                     |

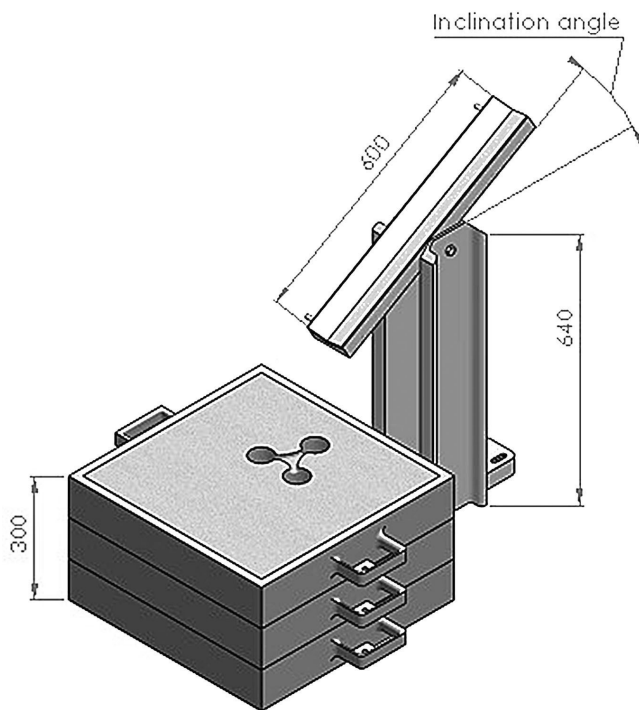


**Figure 1.** Model of the used cooling plate and the mold.

The temperature measuring equipment is an S type thermocouple fixed at the start point of the cooling plate. The used furnace is an electrical induction furnace with a total capacity of 90 kg of the cast material and power of 200 kW. The furnace can swivel easily in order to pour the molten metal into the ladle. The molten metal have to reach a superheat of 1400 °C in the furnace before cooling down in the ladle to reach the required pouring temperature. Before pouring the molten metal above the cooling plate a specimen is taken to ensure the required chemical composition. The mold is prepared to obtain three test specimens. The used mold material is silica sand. The required test specimen pattern dimensions takes in consideration the casting allowances, *Figure 2*. There is no complex gating system in this mold according to the low temperature of poured slurry.

A tensile test and Rockwell hardness test is performed on the specimens to investigate the mechanical properties. The tensile test specimen dimensions are taken according to DIN 1561 and the results are tabulated to make comparisons between specimens. Microstructural investigations are carried out using an optical microscope. The used etchant is Nital (98 mL ethanol and 4 mL nitric acid) ac-

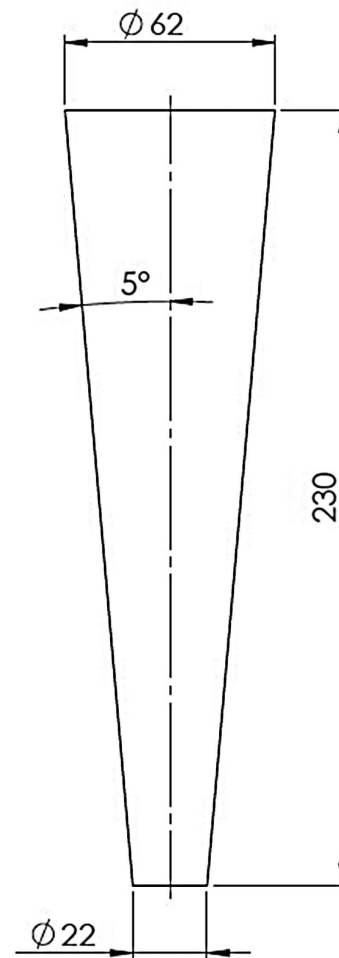


**Figure 2.** Drawing of the casted specimen.

ording to ASM handbook vol. 9 [7]. The microstructural measurements of the carbon particles size and circularity were performed using image analyzing techniques software “jmicrovision”.

## 3 Results and discussion

### 3.1 Microstructural examination

There are three tested regions of the specimen in the microstructural examination, *Figure 3*. The microstructure of the center of specimen A with a 100x magnification clarifies that the carbon particles have the shape of flakes with sharp edges which increases micro cracking, *Figure 4*. The effect of micro cracks in cast iron is investigated elsewhere [8]. For specimen A the shearing action of slope cooling doesn't affect the carbon morphology as well if

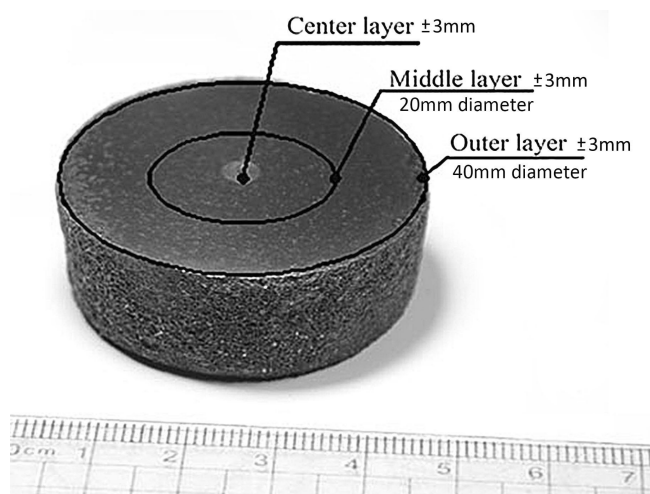


**Figure 3.** Tested regions of the specimens.

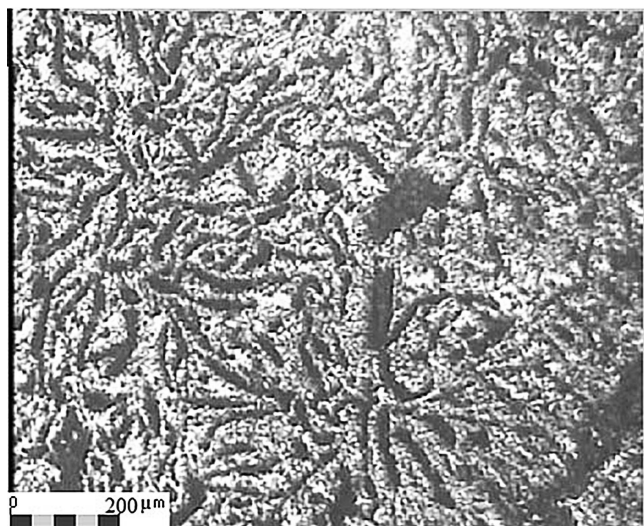


**Figure 4.** Microstructure of specimen A in the center.

compared with the other specimens. On the other hand there are particles of graphite with less sharp edges and starting to be round in shape when getting closer to the specimens center, *Figure 5*. Then the graphite particles are turned into round shapes with a small particle size at the specimen's center, *Figure 6*.

The change in particle size relative to region of the microstructure is illustrated, *Figure 7*. From the graph it is clear that the particle size is decreased when getting near to the outer layer of the specimen with an increase in the particles count. The results indicate that there is an inversely proportional relation between the carbon particles size and count following the equation (2).

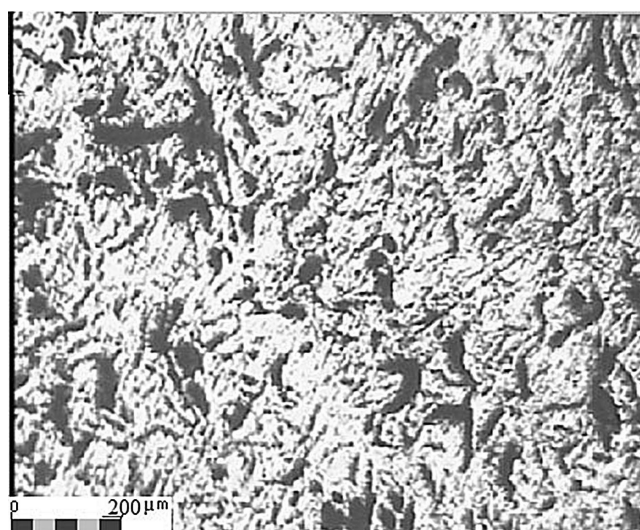


**Figure 5.** Microstructure of specimen A in the middle.

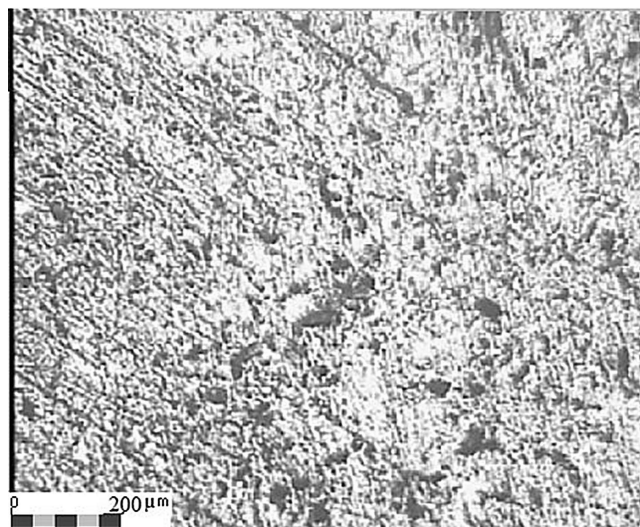


**Figure 6.** Microstructure of specimen A in the outer layer.

$$P_c = 332.99 e^{-0.015 P_s} \quad (2)$$

where ' $P_c$ ' is the particles count and ' $P_s$ ' is the particles size with a correlation factor ' $R^2$ ' value of 0.9956. This change in carbon particle size usually results from the higher cooling rate of the outer layer of casting compare to the center layer. The particle size measuring method is according to "Grain size measurement by image analysis" by Diógenes A. N., et al [9]. Every microstructure image are filtered to get the best results, *Figure 8*. To measure the needed parameters from the JMicrovision program the configurations are set to get a selection of all carbon particle shapes, *Table 2*.

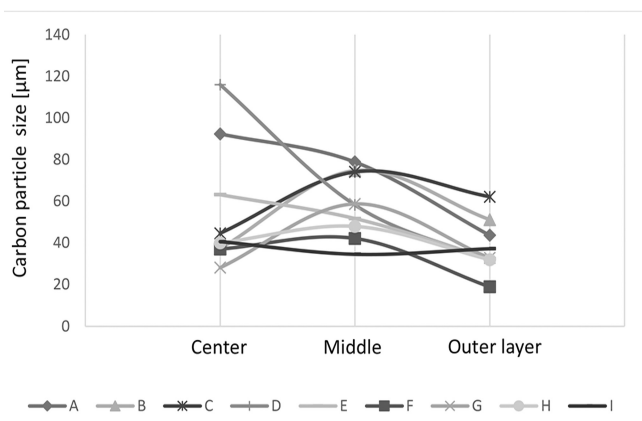


**Figure 7.** The change in carbon particle size relative to region of the microstructure.

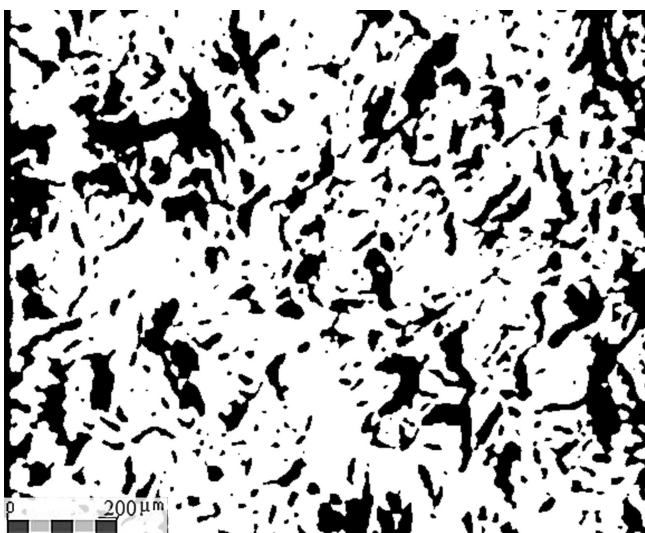


**Figure 8.** Resulting image after filtering processes for the middle layer of specimen A.

Another measure of the carbon particle morphology is the particle circularity which indicates that the carbon particle shape is flakes or circular, *Table 3*. The change in circularity with respect to the

region of the microstructure is illustrated, *Figure 9*. The circularity measuring method is according to “Particle Shape Factors and Their Use in Image Analysis” [10]. The image processing software ‘JMicrovision’ helps evaluating the area and perimeter of the carbon particle to be substituted in equation (3). The circularity number for each specimen is the average of the calculated particles circularity numbers.

$$\text{Average Circularity} = \frac{\sum_{i=1}^n \sqrt{\frac{4\pi A}{P^2}}}{n} \quad (3)$$

where: ‘A’ is the area of each carbon particle in the specimen, ‘P’ is the perimeter of each carbon particle in the specimen, and ‘n’ is the number of measured carbon particles in the specimen. The circularity of carbon particles increases when getting closer to the outer layer of specimen, *Figure 9*. This is seems to be happening according to the cooling rate differences between the center and the outer layer and the mechanical shear on the semi-solid slurry layers due to the friction between the semi-solid slurry and the mold wall. There are some specimens behaved differently in their circularity changes along the specimen’s tested region. To know the real effect of changing the specimens tested region the average circularity for the specimens is analyzed using Taguchi’s method by the Minitab program. The signal to noise (S/N ratio) which is the ratio of the mean “signal” to the standard deviation “noise” is increasing when getting closer to the outer layer but the trend line slope between the center and middle layers ratios is very small, which indicates that the circularity improvement between these layers are intangible, *Figure 10*.

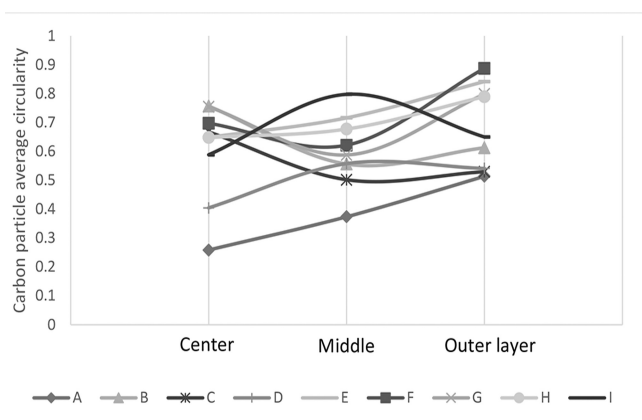
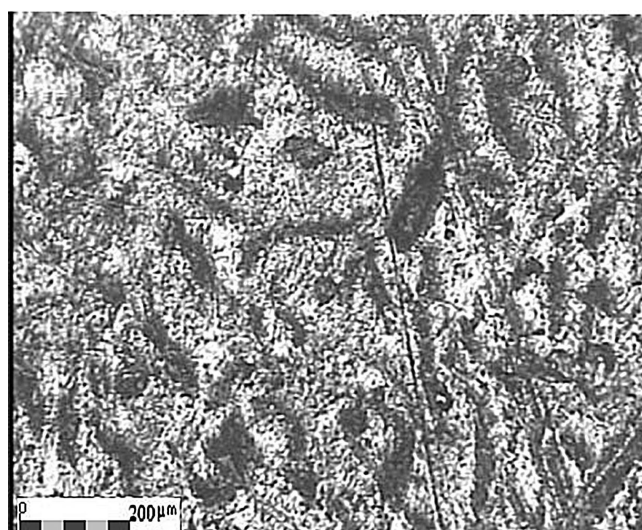
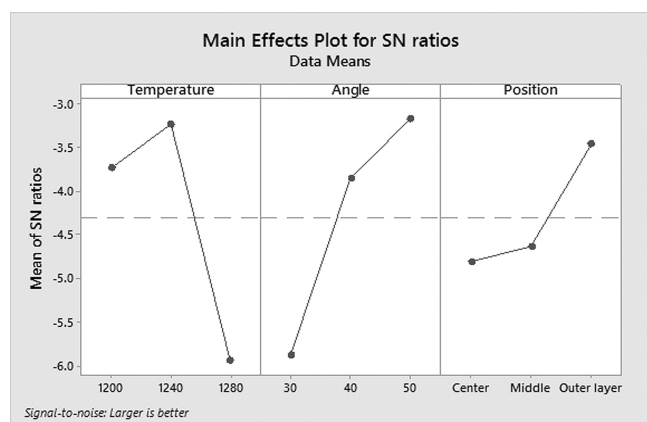
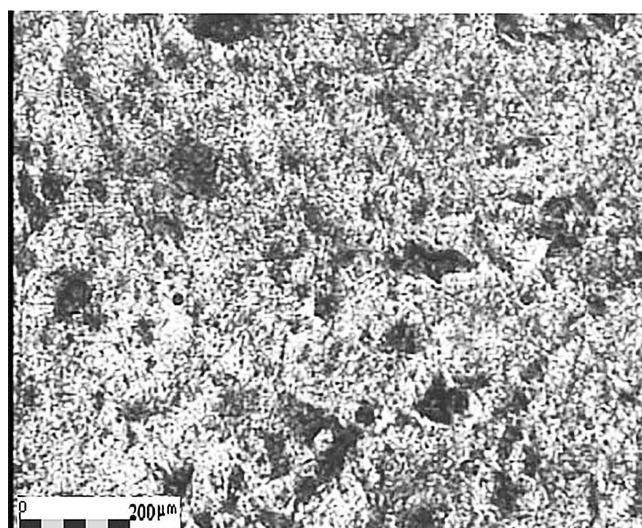
The microstructure of the middle layer of the specimens (G, H, and I) which have the same cool-

**Table 2.** Settings for JMicrovision program for objects extraction.

|                   |                                     |                             |
|-------------------|-------------------------------------|-----------------------------|
| Object separation | Max cut length (pixels)             | 25                          |
|                   | Max cut angle (degrees)             | 130                         |
|                   | Min inter object perimeter (pixels) | 10                          |
|                   | Outline approximation (pixels)      | 10                          |
| Shape size        | Min shape size (μm)                 | Height = 3.5<br>Width = 4.6 |
|                   | Max shape size (μm)                 | Height = 6.5<br>Width = 8.5 |

**Table 3.** Carbon particles size and circularity for specimens.

| Code | Carbon particle average size [ $\mu\text{m}$ ] |        |             | Carbon particle average circularity |        |             |
|------|--|--------|-------------|-------------------------------------|--------|-------------|
|      | Center   | Middle | Outer layer | Center                              | Middle | Outer layer |
| A    | 4.615  | 3.94   | 2.181       | 0.258                               | 0.373  | 0.514       |
| B    | 1.864  | 3.736  | 2.557       | 0.757                               | 0.556  | 0.612       |
| C    | 2.229  | 3.703  | 3.107       | 0.668                               | 0.501  | 0.529       |
| D    | 5.796  | 2.908  | 1.579       | 0.404                               | 0.558  | 0.541       |
| E    | 3.158  | 2.585  | 1.625       | 0.648                               | 0.716  | 0.842       |
| F    | 1.852  | 2.107  | 0.944       | 0.697                               | 0.621  | 0.888       |
| G    | 1.404  | 2.934  | 1.637       | 0.754                               | 0.587  | 0.798       |
| H    | 2.001  | 2.396  | 1.596       | 0.648                               | 0.677  | 0.789       |
| I    | 2.028  | 1.729  | 1.861       | 0.588                               | 0.797  | 0.65        |

**Figure 9.** The change in circularity with respect to the region of the microstructure.**Figure 11.** Microstructure for middle layer of specimen G.**Figure 10.** The S/N ratio for the change in circularity with respect to the region of the microstructure pouring temperature and inclination angle.**Figure 12.** Microstructure for middle layer of specimen H.

ing plate inclination angle of  $50^\circ$  and different pouring temperatures is shown with 100x magnification, Figures 11, 12, 13. These microstructures show that

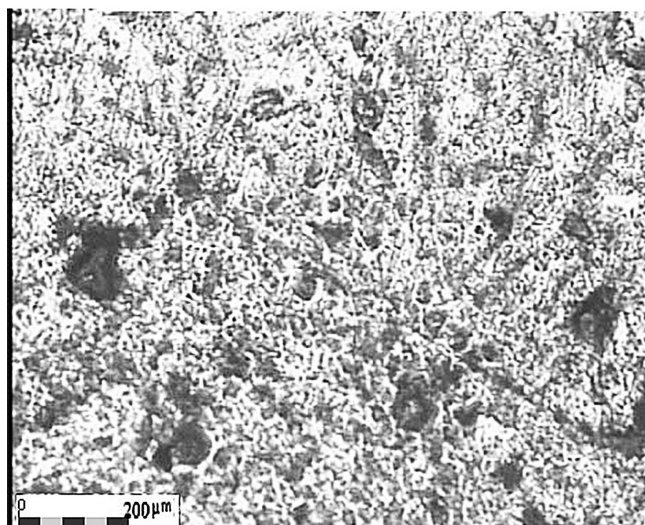


**Figure 13.** Microstructure for middle layer of specimen I.

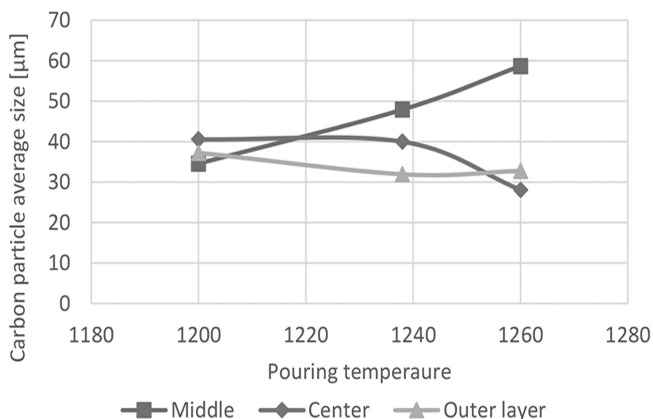


**Figure 14.** Relation between carbon particle size and pouring temperature for specimens with 50° cooling plate inclination.

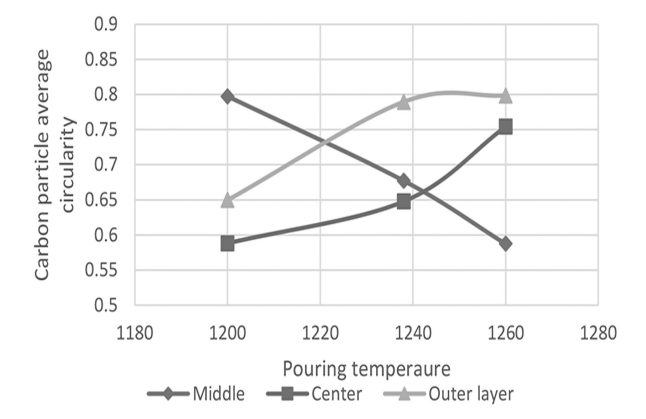


**Figure 15.** Relation between carbon particle circularity and pouring temperature for specimens with 50° cooling plate inclination.

the decrease of pouring temperature affects the carbon particles shearing to produce shapes of carbon with better circularity, *Figure 14, 15.*

The particle size is increasing with the increase of pouring temperature in the middle layer of specimen, *Figure 14.* On the other hand there is a decrease of the particle circularity with the increase of the pouring temperature at the middle of the specimen, *Figure 15.* But for the center and the outer layer there are changes in the behavior of the curves. For the middle of the specimen at the high temperature condition the carbon particles can be easily formed due to the long diffusion process until it solidifies. Thus these carbon particles are able to grow more than those of lower temperature conditions. The decrease of circularity may result from the poor shearing action on the semi-solid slurry of metal passing over the plate at high pouring temperature. Also the metal can flow over the plate before the formation of the carbon solid particles. As a result there is a smaller shearing acting on the carbon particles. On the other hand for the outer layer of specimens the friction between the mold wall and the semi-solid slurry affects on the carbon particles morphology so the results varies from those in the middle layer and center layer of the specimen. This result appears clearly in the S/N ratio plot. The ratio of the outer layer of specimens is very high if compared with that for the middle and center layers, *Figure 10.* As an estimation the bottom of the specimen which only has a 20 mm casting wall thickness has a better circularity for its rapid cooling. The regression equation (4) for the particles circularity helps in predicting the circularity for the bottom of the specimens with an ‘R2’ value of 41.58 %.

$$\text{Particle circularity} = 2.234 - 0.001600\text{Temperature} + 0.00844\text{Angle} + 0.00206\text{layer diameter} \tag{4}$$

The microstructure of the middle layer of the specimens (H, B, and E) is investigated in this work to investigate the influence of the inclination angle, *Figure 12, Figure 16, 17.* These microstructures show a change in the carbon particles shape that the particles in specimen ‘B’ is the flak shape then the circularity becomes larger in specimen ‘E’ and the largest circularity is in specimen ‘H’. The S/N ratio plot for the inclination angle effect ensures these indications, *Figure 10.* The change in particle size and

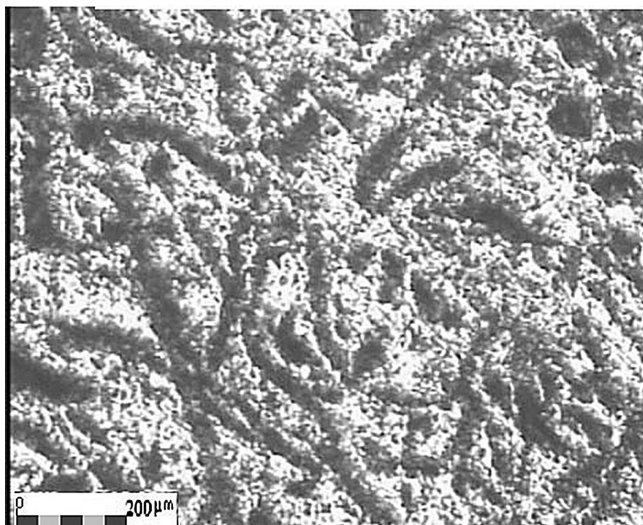


**Figure 16.** Microstructure for middle layer of specimen B.

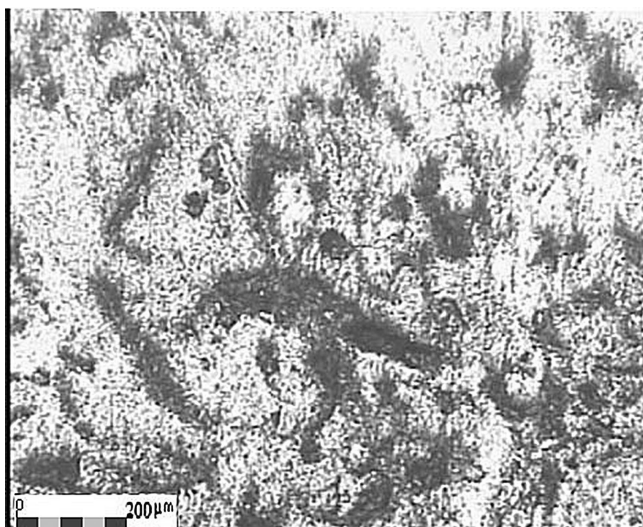


**Figure 17.** Microstructure for middle layer of specimen E.

circularity with the inclination angle is very clear for the medium pouring temperature, *Figure 18, 19*. The results show that the best conditions for the particles circularity is the medium pouring temperature, 50° inclination angle, and the outer layer of specimens.

### 3.2 Mechanical properties

The application of the cooling slope technique to the casting of the specimen affected clearly on its mechanical properties. Every specimen has a three copies to get an average result of the tensile test.

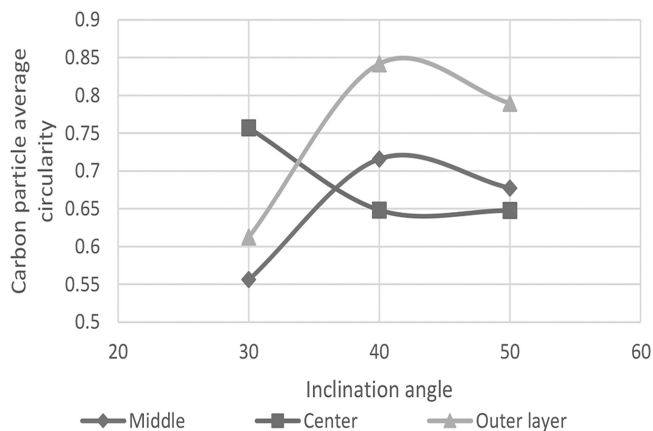


**Figure 18.** Relation between carbon particle circularity and inclination angle for specimens with medium pouring temperature.

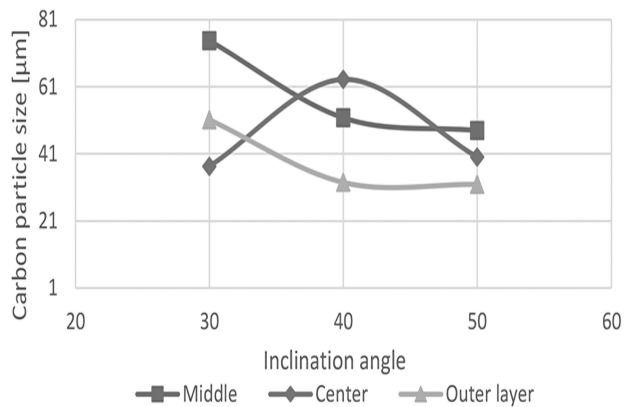


**Figure 19.** Relation between carbon particle size and inclination angle for specimens with medium pouring temperature.

The tensile test results show that the highest value of the ultimate tensile strength ( $\sigma_u$ ) appears in specimen A, *Table 4*. This result indicates that the highest pouring temperature of specimen A makes it the best in the ultimate tensile strength values although it has the least value of carbon particle circularity. The high pouring temperature of specimens A, D, and G makes the feeding of the mold during casting easier. This action results in a lower count of porosities and defects compared with those of other specimens, *Figure 20*. The tensile test results and its' S/N ratio (larger is better) plot show that the increase of pouring temperature and the decrease in inclination angle improved the ultimate tensile strength of the specimens, *Figures 21-23*.



**Table 4.** Ultimate tensile strength values

| Specimen code           | A      | B      | C      | D      | E      |
|-------------------------|--------|--------|--------|--------|--------|
| Ultimate strength [MPa] | 186.13 | 183.15 | 162.27 | 175.59 | 167.84 |
| Specimen code           | F      | G      | H      | I      |        |
| Ultimate strength [MPa] | 155.71 | 163.06 | 160.88 | 152.52 |        |

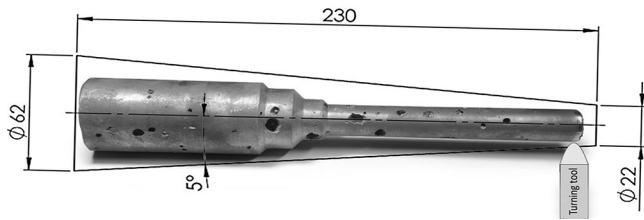


**Figure 20.** Defects in “C” specimen after machining.

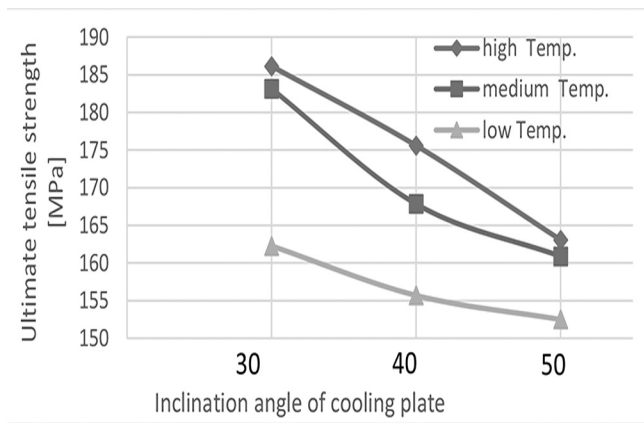


**Figure 21.** Relation between ultimate tensile strength [MPa] and the inclination angle for Specimens.

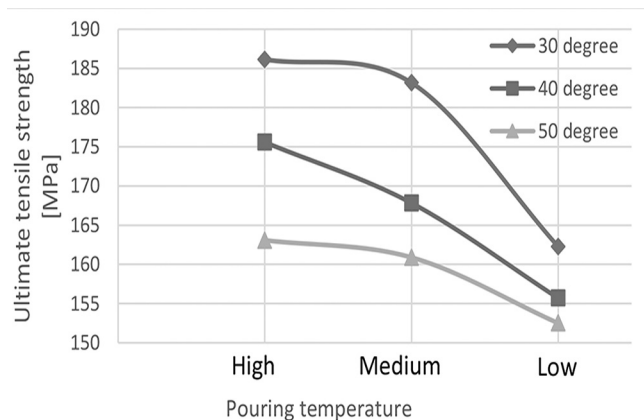


**Figure 22.** Relation between ultimate tensile strength [MPa] and the pouring temperature for specimens.

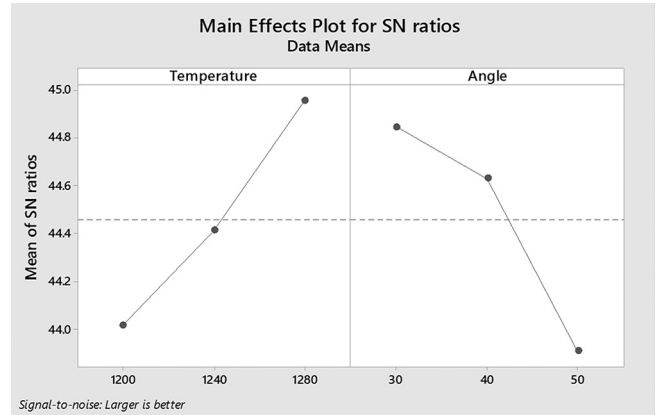


**Figure 23.** S/N ratio for the change in strength with respect to the pouring temperature and inclination angle.

The values of Rockwell hardness numbers (HRC) of the tested specimens and its relation with the position of the tested region indicates that the outer layer of each specimen is harder than the inner layers, Table 5, Figure 24, 25. This is because of the small size of carbon particles, the rapid cooling during solidification, and the large circularity number of the carbon particles.

**Table 5.** Rockwell hardness numbers of specimens.

| code | Outer layer | HRC Middle layer | Center |
|------|-------------|------------------|--------|
| A    | 91          | 83               | 70     |
| B    | 89          | 84               | 78     |
| C    | 89          | 86               | 85     |
| D    | 86          | 84               | 83     |
| E    | 95          | 86               | 84     |
| F    | 91          | 86               | 78     |
| G    | 92          | 84               | 80     |
| H    | 91          | 87               | 85     |
| I    | 88          | 82               | 80     |

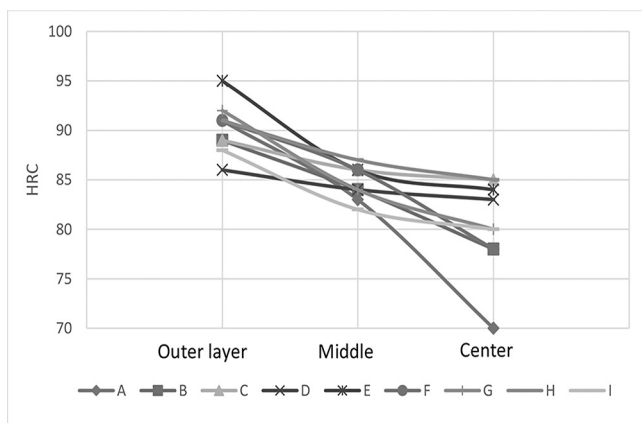


**Figure 24.** Relation between the Rockwell hardness number and the tested region position.

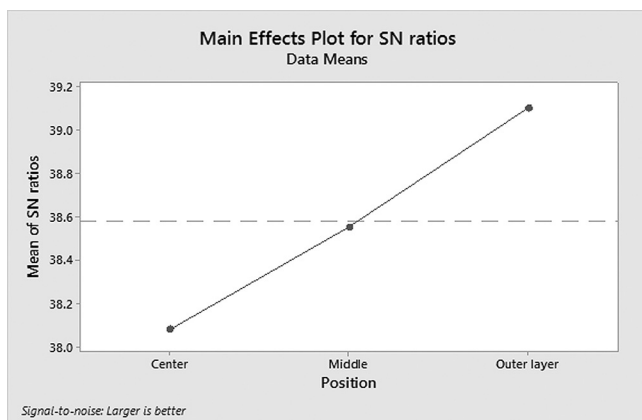


**Figure 25.** S/N ratio for the change in hardness with respect to position of the tested region.

## 4 Conclusions

From the microstructural examination it is noticed that slope cooling casting improved the shape of the carbon particles existed in the grey cast iron microstructure. When using a smaller inclination angle of the cooling plate the shearing action gets higher resulting in a fine microstructure. For low pouring temperature conditions the porosities are increased producing a small tensile strength. The carbon particle morphology varies along the specimen layers

that its size increases and circularity decreases when getting closer to the center of the specimen. The cooling rate affects the carbon particles size and shape during the slope cooling process that the high cooling rate during the process enhances the mechanical shear of carbon particles but increases the casting porosities.

## Acknowledgements

The authors acknowledge the Faculty of Engineering at Shoubra - Benha University for providing facilities, the Central Metallurgical Research and Development Institute Centre, Cairo, Egypt for casting the specimens, and Modern Academy for Engineering and Technology, Cairo, Egypt for performing the tests on the specimens.

## 5 References

- [1] R. Singh, *Mater. Perform.* **2009**, 58–61.
- [2] A. F. S., *The Cupola and Its Operation*, Illinois **1954**.
- [3] S. Tiwari, *Cast Iron Technology*, CBS Publishers & Distributers, New Delhi **2007**.
- [4] Z. Fan, *Int. Mater. Rev.*, **2002**, 47, 49.
- [5] A. Muumbo, M. Takita, H. Nomura, *Mater. Trans.* **2003**, 44, 893.
- [6] M. Ramadan, M. Takita, H. Nomura, *Mater. Sci. Eng. A*, **2006**, 417, 166.
- [7] J. Radzikowska, *ASM Handb. Metallogr. Microstruct.* **2004**, 9, 565.
- [8] G. Zambelli, *Gruppo Italiano Frattura*, **1980**, 227.
- [9] A. N. Diógenes, E. Hoff, C. P. Fernandes, *ABCM*, **2005**, 5.
- [10] E. Olson, *Journal of GXP Compliance*, **2011**, 15, 85.

Received in final form: April 17<sup>th</sup> 2017